Nonequilibrium Analysis Alters the Mechanistic Interpretation of Inhibition of Acetylcholinesterase by Peripheral Site Ligands†

Tivadar Szegletes, William D. Mallender, and Terrone L. Rosenberry*

Department of Pharmacology, Mayo Foundation for Medical Education and Research, and Department of Research, Mayo Clinic Jacksonville, Jacksonville, Florida 32224

Received August 29, 1997; Revised Manuscript Received November 13, 1997

ABSTRACT: The active site gorge of acetylcholinesterase (AChE) contains two sites of ligand binding, an acylation site near the base of the gorge with a catalytic triad characteristic of serine hydrolases, and a peripheral site at the mouth of the gorge some 10−20 Å from the acylation site. Many ligands that bind exclusively to the peripheral site inhibit substrate hydrolysis at the acylation site, but the mechanistic interpretation of this inhibition has been unclear. Previous interpretations have been based on analyses of inhibition patterns obtained from steady-state kinetic models that assume equilibrium ligand binding. These analyses indicate that inhibitors bound to the peripheral site decrease acylation and deacylation rate constants and/or decrease substrate affinity at the acylation site by factors of up to 100. Conformational interactions have been proposed to account for such large inhibitory effects transmitted over the distance between the two sites, but site-specific mutagenesis has failed to reveal residues that mediate the proposed conformational linkage. Since examination of individual rate constants in the AChE catalytic pathway reveals that assumptions of equilibrium ligand binding cannot be justified, we introduce here an alternative nonequilibrium analysis of the steady-state inhibition patterns. This analysis incorporates a steric blockade hypothesis which assumes that the only effect of a bound peripheral site ligand is to decrease the association and dissociation rate constants for an acylation site ligand without altering the equilibrium constant for ligand binding to the acylation site. Simulations based on this nonequilibrium steric blockade model were in good agreement with experimental data for inhibition by the peripheral site ligands propidium and gallamine at low concentrations of either acetylthiocholine or phenyl acetate if binding of these ligands slows substrate association and dissociation rate constants by factors of 5−70. Direct measurements with the acylation site ligands huperzine A and *m*-(*N*,*N*,*N*-trimethylammonio)trifluoroacetophenone showed that bound propidium decreased the association rate constants 49- and 380-fold and the dissociation rate constants 10- and 60-fold, respectively, relative to the rate constants for these acylation site ligands with free AChE, in reasonable agreement with the nonequilibrium steric blockade model. We conclude that this model can account for the inhibition of AChE by small peripheral site ligands such as propidium without invoking any conformational interaction between the peripheral and acylation sites.

Acetylcholinesterase (AChE)[1] hydrolyzes its physiological substrate acetylcholine at one of the highest known catalytic rates (*1*), and the unique features of AChE structure that determine its catalytic power have been pursued for many years. A major advance occurred with the X-ray crystallographic determination of the three-dimensional structure of *Torpedo californica* AChE (TcAChE) (*2*). This structure revealed an active site gorge lined with aromatic residues that is about 20 Å deep. Two sites of ligand interaction in AChE were first demonstrated in ligand binding studies (*3*) and later confirmed by crystallography, site-specific mutagenesis, and molecular modeling: an *acylation site* at the base of the gorge and a *peripheral site* at its mouth. In the acylation site (Figure 1) residue S200 (TcAChE sequence numbering) is acylated and deacylated during substrate turnover, H440 and E327 participate with S200 in a catalytic triad (E−H−S), and W84 binds to the trimethylammonium group of acetylcholine as acyl transfer to S200 is initiated. The peripheral site involves other residues including W279 (*4*−*9*). Ligands can bind selectively to either the acylation or the peripheral sites, and ternary complexes with distinct ligands bound to each site can form (*3*). Peripheral site ligands that form these ternary complexes include the

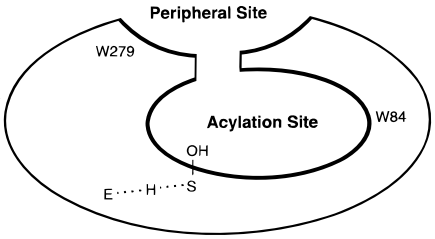

FIGURE 1: Schematic diagram of the sites for ligand binding in AChE.

† This work was supported by Grant NS-16577 from the National Institutes of Health and by grants from the Muscular Dystrophy Association of America. W.D.M. was supported by a Kendall-Mayo Postdoctoral Fellowship.

* To whom correspondence should be addressed.

[1] Abbreviations: AChE, acetylcholinesterase; TcAChE, acetylcholinesterase from *Torpedo californica*; DTNB, 5,5′-dithiobis(2-nitrobenzoic acid); TMTFA, *m*-(*N*,*N*,*N*-trimethylammonio)trifluoroacetophenone.

S0006-2960(97)02158-2 CCC: $15.00
Published on Web 03/05/1998

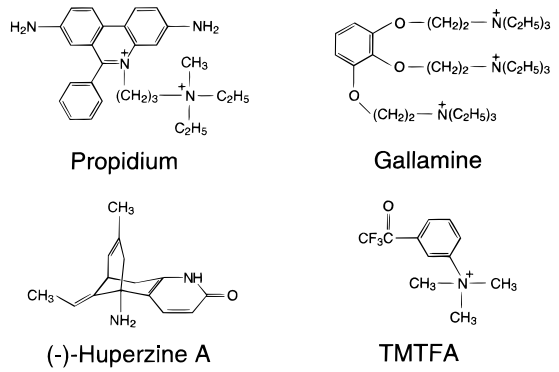

FIGURE 2: Structures of peripheral site and acylation site ligands.

phenanthridinium derivative propidium (Figure 2) and the fasciculins, a family of very similar snake venom neurotoxins composed of 61-amino acid polypeptides (*10*, *11*).

In this paper we address the question of how ligand binding to the peripheral site alters AChE catalytic activity. While it is well documented that ligand binding to this site can inhibit substrate hydrolysis, the mechanism of this inhibition is less clear. Specifically, an understanding of the inhibition mechanism may depend on whether the substrate and inhibitor are equilibrated with AChE. This point can be examined in the conventional pathway for the hydrolysis of acetylcholine (S) by AChE (*E*) in Scheme 1.[2] The initial

Scheme 1

$$E + S \underset{k_{-S}}{\overset{k_S}{\rightleftharpoons}} ES \xrightarrow{k_2} EA \xrightarrow{k_3} E + P$$

enzyme−substrate complex *E*S proceeds to an acylated enzyme intermediate *E*A which is then hydrolyzed to product P and *E* (see ref *12*). Under classical steady-state conditions (*13*), hydrolysis rates v vary with [S] according to the Michaelis−Menten equation (eq 1a) to give the maximum hydrolysis rate V_{max}, the apparent first-order rate constant k_{cat}, and the second-order rate constant k_{cat}/K_{app} (eqs 1b and 1c).

$$v = \frac{d[P]}{dt} = \frac{V_{max}[S]}{[S] + K_{app}} \quad (1a)$$

$$\frac{V_{max}}{[E]_{tot}} = k_{cat} = \frac{k_2 k_3}{k_2 + k_3} \qquad \frac{k_{cat}}{K_{app}} = \frac{k_S k_2}{k_{-S} + k_2} \quad (1b, 1c)$$

One way in which AChE has optimized these rate constants is by accelerating the acylation step k_2 so that it exceeds k_{cat} (eq 1b), which for AChE is about 10^4 s^{-1} (*1*). Of more importance to the arguments here, k_2 also exceeds k_{-S} (*1*, *14*). As a result, *E*S is not in equilibrium with *E* and S. The failure of *E*S to equilibrate with *E* and S is readily accommodated by eq 1c: k_{cat}/K_{app} approaches k_S, the substrate association rate constant. However, when an inhibitor binds to the nonequilibrated *E*S intermediate, the steady-state inhibition patterns present a greater challenge. The conventional interpretation of the classic noncompetitive inhibition pattern, for example, assumes that *E*S is equilibrated (see ref *15*). We avoid this equilibrium assumption here for the first time in the AChE literature by solving the appropriate differential rate equations with the simulation program SCoP. In particular, we examine the simple hypothesis that the only effect of peripheral site inhibitors such as propidium is to impose a steric blockade that decreases association and dissociation rate constants for substrates without altering their ratio, the equilibrium association constant. We test this hypothesis also by examining the effect of peripheral site ligands on the rate constants for the binding of acylation site inhibitors. Our results indicate that failure to achieve equilibrium can have a profound impact on the classical interpretation of AChE inhibition and indeed alter mechanistic conclusions.

EXPERIMENTAL PROCEDURES

Materials. Human erythrocyte AChE was purified as outlined previously and active site concentrations were determined by assuming 410 units/nmol (*16*, *17*). (−)-Huperzine A and propidium iodide were purchased from Calbiochem and gallamine triethiodide from Aldrich Chemical Co. Huperzine A concentrations were adjusted with an extinction coefficient[3] $\epsilon_{308\ nm} = 10400\ M^{-1}\ cm^{-1}$. TMTFA was kindly provided by Dr. Daniel Quinn (University of Iowa), and stock TMTFA concentrations were calibrated by titration with AChE.

Steady-State Measurements of AChE-Catalyzed Substrate Hydrolysis. Hydrolysis rates v were measured at various substrate (S) concentrations in buffer composed of 20 mM sodium phosphate and 0.02% Triton X-100 at pH 7.0 and 25 °C unless otherwise indicated. Acetylthiocholine assay solutions (1 mL) included 0.33 mM DTNB, and hydrolysis was monitored by formation of the thiolate dianion of DTNB at 412 nm ($\Delta\epsilon_{412\ nm} = 14.15\ mM^{-1}\ cm^{-1}$ (*18*)) for 1−5 min on a Varian Cary 3A spectrophotometer (*19*). Acetylthiocholine concentrations were low enough (<0.5 mM) in the absence of inhibitors (*20*) that compensation for substrate inhibition was unnecessary. Hydrolysis rates for phenyl acetate (0.2−5 mM, ≤1% methanol final) were measured in 1-ml assay solutions at 270 nm ($\Delta\epsilon_{270\ nm} = 1.40\ mM^{-1}\ cm^{-1}$) for 1−5 min (*21*). Reciprocal plots of v^{-1} vs $[S]^{-1}$ at all inhibitor (I) concentrations here were linear, and slopes and intercepts of these plots were calculated by weighted linear regression analyses which assumed that v has a constant percent error. Nonlinear regression analyses of these slopes and intercepts vs [I] were conducted with Fig.P (BioSoft, version 6.0) as described, with slope and intercept values weighted by the reciprocal of their variance (also see ref *22*).

Simulations of Kinetic Equations. When the reversible reactions in Scheme 2 below are not at equilibrium, the corresponding differential equations were solved with the program denoted SCoP (version 3.51) developed at the NIH National Center for Research Resources and available from Simulation Resources, Inc. (Berien Springs, MI). A model file was constructed with differential equations for each enzyme intermediate except *E* and with values of all rate constants. Mass conservation was introduced by substitution of $[E] = [E]_{tot} - \Sigma[M]$, where $[E]_{tot}$ is the total concentration

[2] Scheme 1 assumes substrate concentrations low enough that *E*SS or *E*AS species leading to substrate inhibition are negligible (see ref *1*).

[3] Personal communication from B. P. Doctor, Walter Reed Army Institute of Research, Washington, DC.

Table 1: Inhibition of AChE-Catalyzed Hydrolysis of Acetylthiocholine by Propidium[a]

case	k_S (μM^{-1} s^{-1})	k_{-S} (s^{-1})	k_2, k_3 (s^{-1})	k_I (μM^{-1} s^{-1})	k_{-I} (s^{-1})	k_{S2} (μM^{-1} s^{-1})	k_{-S2} (s^{-1})	K_{app}[b] (mM)	slope		intercept
									K_I[b] (μM)	α[b]	β[b]
1	**200**	**3×10^3**	**1.4×10^4**	**200**	**200**	**3**	**45**	0.043	1.00	0.0197	0.09 ± 0.01
2	200	3×10^3	1.4×10^4	200	200	**0.3**	**4.5**	0.043	1.01	0.0033 ± 0.0001	0.030 ± 0.001
3	200	3×10^3	1.4×10^4	200	200	**200**	**3×10^3**	0.043		1.00	1.00
4	200	**3×10^5**	1.4×10^4	200	200	**3**	**4.5×10^3**	0.79	1.00	0.26	0.78 ± 0.05
5	200	**3×10^7**	1.4×10^4	200	200	3	**4.5×10^5**	75	1.00	0.97	1.00

[a] Simulations for cases 1−5 were generated as outlined in the text with indicated rate constant values. Bold entries indicate a change from the previous case. Values of K_{app}, K_I and α and β were calculated by weighted least-squares analysis of replots as in Figure 4. [b] Standard errors were less than 2% of the mean unless otherwise indicated.

of enzyme and Σ [M] is the sum of the concentrations of all enzyme intermediates. An analogous mass conservation was introduced for [S]. Simulation and curve-fitting files were generated by SCoP from the model file by employing the numerical solver clsoda. This solver for stiff and nonstiff sets of differential equations uses an improved Gear method (*23*, *24*).

Rate constants used in these simulations (see Tables 1 and 2) were justified as follows. For acetylthiocholine, direct estimates of k_2 and k_3 (available only for eel AChE) gave $k_2/k_3 = 1.3$ (*25*). Noting a 2-fold smaller k_{cat} of 7000 s^{-1} for human AChE (*26*) and assuming $k_2 = k_3$ for this enzyme, substitution into eq 1b gave $k_2 = k_3 = 1.4 \times 10^4$ s^{-1}. Solvent deuterium oxide (D_2O) isotope effects provided an estimate of k_{-S}: k_{cat} for acetylthiocholine was slowed by a factor of 2.03 ± 0.05 when H_2O was replaced by D_2O, a value close to a typical factor of 2.5 for enzyme-catalyzed steps that are rate limited by proton transfer (*14*), but k_{cat}/K_{app} decreased by a factor of only 1.21 ± 0.02 in D_2O (*22*). Inserting this value in eq 1c and assuming that k_2 decreased by a factor of 2.5 in D_2O while k_S and k_{-S} were unaffected, then $k_2/k_{-S} = 6$ and, from k_2 above, $k_{-S} = 3 \times 10^3$ s^{-1}. An estimate of $k_S = 2 \times 10^8$ M^{-1} s^{-1} was obtained by substitution of these values of k_2 and k_{-S} and the observed value of $K_{app} = 45$ μM (see Table 2) into eq 1c. For phenyl acetate, k_{cat} was assumed equal to that of acetylthiocholine (*1*) and the same value of 1.4×10^4 s^{-1} was assigned for k_2 and k_3. From observed D_2O isotope effects of 2.45 ± 0.08 for k_{cat} and 1.48 ± 0.05 for k_{cat}/K_{app} (*22*), k_2 was assumed to decrease by a factor of 2.5 in D_2O while k_S and k_{-S} were unaffected, yielding $k_2/k_{-S} = 2.1$ and $k_{-S} = 7 \times 10^3$ s^{-1}. These values together with the observed value of $K_{app} = 1.31$ mM (see Table 2) gave $k_S = 8 \times 10^6$ M^{-1} s^{-1} for phenyl acetate from eq 1c. For propidium and gallamine, an estimate of $k_I = 2 \times 10^8$ M^{-1} s^{-1} was based on association rate constants of 5×10^7 M^{-1} s^{-1} for the bisquaternary ligand ambenonium (*20*) and 4×10^8 M^{-1} s^{-1} for *N*-methylacridinium (*27*) with human AChE. Values for k_{-I} were then calculated from $k_{-I} = (k_I)(K_I)$, where K_I was the observed equilibrium inhibition constant for propidium or gallamine (see Table 2).

Slow Equilibration of an Acylation Site Ligand in the Presence of a Peripheral Site Inhibitor. The slow interaction of an acylation site ligand (L) with AChE in the presence of a peripheral site inhibitor I as shown in Scheme 3 in the Results was analyzed by procedures used previously (*22*) to describe the interaction of fasciculin 2 with AChE. Bovine serum albumin (1 mg/mL) was incubated overnight in buffer (20 mM sodium phosphate, 0.02% Triton X-100, pH 7.0) containing 0.33 mM 5,5′-dithiobis(2-nitrobenzoic acid) (DTNB), and association reactions were initiated by adding AChE, the inhibitor propidium, and the acylation site ligand (huperzine A or TMTFA) at 23 °C. Except where indicated, binding was measured under pseudo-first-order conditions in which the concentration of ligand was adjusted to at least 10 times the concentration of AChE. At various times a 1.0-mL aliquot was removed to a cuvette, 40 μL of acetylthiocholine and DTNB were added to final concentrations of 0.5 mM and 0.33 mM, respectively, and a continuous assay trace was immediately recorded at 412 nm. Background rates in the absence of AChE were subtracted. Dissociation reactions were measured by incubating ligand with AChE for 1−24 h, diluting ≥200-fold to the indicated final concentrations, and assaying 1.0-mL aliquots as above.

Assay rates v from association and dissociation reactions of huperzine A and TMTFA were divided by control assay rates in the absence of these ligands ($v_{H=0}$ or $v_{TMTFA=0}$) to give a normalized value $v_{(N)}$. For huperzine A these values were fitted by nonlinear regression analysis (Fig.P) to eq 2, where $v_{(N)initial}$ and $v_{(N)final}$ are the calculated values of $v_{(N)}$ at time zero and at equilibrium, respectively, and the observed

$$v_{(N)} = v_{(N)final} + (v_{(N)inital} - v_{(N)final})e^{-kt} \qquad (2)$$

pseudo first-order rate constant k for the approach to equilibrium is given by eq 3.

$$k = k_{on}[L] + k_{off} \qquad (3)$$

In eq 3,

$$k_{on} = \frac{k_L + k_{L2}\frac{[I]}{K_I}}{1 + \frac{[I]}{K_I}} \qquad k_{off} = \frac{k_{-L} + k_{-L2}\frac{[I]}{K_{LI}}}{1 + \frac{[I]}{K_{LI}}} \qquad (4a, 4b)$$

Structure Analysis and Molecular Graphics. Construction and analysis of three-dimensional models were performed on a Silicon Graphics workstation Indigo2 IMPACT using QUANTA96 modeling software (Molecular Simulations, Inc.). Modeling of the ternary TcAChE enzyme−inhibitor complexes began with the crystal structure coordinates for the TcAChE−huperzine A complex [Protein Data Bank (PDB) file: 1VOT] (*28*) and the TcAChE−TMTFA complex (PDB file: 1AMN) (*29*). Propidium was manually docked into the peripheral site as previously described (*7*). Briefly, the aromatic and alkyl portions of propidium were positioned in the peripheral site and active site gorge by avoiding unfavorable contacts with the TcAChE structure. The resulting structures were optimized by energy minimization

Table 2: Observed and Simulated Inhibition of AChE-Catalyzed Hydrolysis of Acetylthiocholine and Phenyl Acetate by Peripheral Site Ligands[a]

substrate inhibitor	observed parameters				simulated parameters[b]			
	K_{app} (mM)	K_I (μM)	α	β	k_{S2}/k_S	K_I[c] (μM)	α[c]	β
acetylthiocholine	0.045 ± 0.003							
propidium		1.1 ± 0.1	0.019 ± 0.004	0.10 ± 0.01	0.015	1.00	0.0197	0.09 ± 0.01
gallamine		37 ± 2	0.019 ± 0.002	0.44 ± 0.03	0.015	35	0.0189	0.5 ± 0.1
phenyl acetate	1.31 ± 0.15							
propidium		0.8 ± 0.1	0.071 ± 0.008	0.46 ± 0.02	0.05	1.01	0.076	0.4 ± 0.1
gallamine		31 ± 5	0.25 ± 0.01	1.0 ± 0.1	0.2	39	0.27	0.95 ± 0.03

[a] Values of K_{app}, K_I, α, and β were calculated by analysis of replots as in Figures 3 and 4. The ratio of k_{S2}/k_S in each simulation was assigned to give optimal agreement between the observed and simulated parameters. [b] Simulations were conducted with the rate constants from case 1 in Table 1 except as follows: When gallamine replaced propidium, $k_{-I} = 6 \times 10^3$ s^{-1}; when phenyl acetate replaced acetylthiocholine, $k_S = 8$ μM^{-1} s^{-1} and $k_{-S} = 7 \times 10^3$ s^{-1}; with phenyl acetate and propidium, $k_{S2} = 0.4$ μM^{-1} s^{-1} and $k_{-S2} = 350$ s^{-1}; and with phenyl acetate and gallamine, $k_{S2} = 1.6$ μM^{-1} s^{-1} and $k_{-S2} = 1.4 \times 10^3$ s^{-1}. Simulated K_{app} values were identical to the experimental K_{app}, as expected from the assignment of rate constants in Table 1. [c] Standard errors were less than 2% of the mean.

using the CHARMm module of QUANTA96 (conjugate gradient). Initial structural refinement included only the propidium and gorge solvent molecules while final optimization added all amino acid side chains vicinal to propidium and the acylation site ligand.

RESULTS

Equilibrium Model of AChE Inhibition. When ligands bind to the peripheral site, AChE activity is often inhibited. The inhibitor (I) can bind to each of the three enzyme species from Scheme 1, as modeled in Scheme 2. For example, ESI$_P$

Scheme 2

$$\begin{array}{ccccccccc} S & + & E & \underset{k_{-S}}{\overset{k_S}{\rightleftharpoons}} & ES & \xrightarrow{k_2} & EA & \xrightarrow{k_3} & E + P \\ & & + & & + & & + & & \\ & & I & & I & & I & & \end{array}$$

$$k_I \Big\updownarrow k_{-I} \qquad k_{SI} \Big\updownarrow k_{-SI} \qquad k_{AI} \Big\updownarrow k_{-AI}$$

$$S + EI_P \underset{k_{-S2}}{\overset{k_{S2}}{\rightleftharpoons}} ESI_P \xrightarrow{ak_2} EAI_P \xrightarrow{bk_3} EI_P + P$$

represents a ternary complex with S at the acylation site and I at the peripheral site (denoted by the subscript P). The acylation rate constant k_2 is altered by a factor a in this ternary complex, and the deacylation rate constant k_3 is altered by a factor b in the EAI$_P$ complex. To characterize how a peripheral site ligand inhibits AChE, it is useful to know whether substrate affinities are altered and whether the relative rate constants a and b are less than 1 when the inhibitor is bound. Unfortunately, for acetylcholine and other carboxylester substrates, the acylation and deacylation rate constants are too fast to permit direct measurement by any rapid kinetic technique. Consequently, investigations of Scheme 2 have employed steady-state kinetic analyses based on extensions of the Michaelis−Menten expression. However, this approach is problematic. In contrast to the simple steady-state solution in the absence of inhibitor, the general steady-state solution for v in Scheme 2 is too complex for useful comparison to experimental data (*30, 31*). To obtain a more tractable simplified solution, it has invariably been assumed with AChE that the reversible reactions in Scheme 2 are at equilibrium (i.e., $k_{-S} \gg k_2$; $k_{-S2} \gg ak_2$; $k_{-SI} \gg k_2$; $k_{-SI} \gg ak_2$; $k_{-AI} \gg k_3$; $k_{-AI} \gg bk_3$; *32*; *33*; see ref *22*). This solution is given in eq 5, where $K_X = k_{-X}/k_X$.

$$v^{-1} = \frac{1}{V_{max}}\left[\frac{k_{cat}\left(1+\frac{[I]}{K_{SI}}\right)}{k_2\left(1+\frac{a[I]}{K_{SI}}\right)} + \frac{k_{cat}\left(1+\frac{[I]}{K_{AI}}\right)}{k_3\left(1+\frac{b[I]}{K_{AI}}\right)} + \frac{K_{app}\left(1+\frac{[I]}{K_I}\right)}{[S]\left(1+\frac{a[I]}{K_{SI}}\right)}\right] \quad (5)$$

Many inhibition patterns observed with AChE are consistent with eq 5. For example, propidium inhibition of phenyl acetate and acetylthiocholine hydrolysis gave the steady-state kinetic data in Figure 3a,b and Figure 4a,b. The slopes of the reciprocal plots in Figure 3a increased with propidium concentration (Figure 3b), and analyses of these slopes by eq 6 allowed estimation of K_I, the equilibrium dissociation

$$\frac{\text{slope } (v^{-1} \text{ vs } [S]^{-1})}{K_{app}/V_{max}} = \frac{\left(1+\frac{[I]}{K_I}\right)}{\left(1+\frac{\alpha[I]}{K_I}\right)} \quad (6)$$

constant for I with E, and the *experimental* parameter α. At saturating concentrations of I ($[I] \gg K_I/\alpha$), the slope in eq 6 $= K_{app}/\alpha V_{max}$. Therefore, α is simply the ratio of the second-order rate constant with saturating I, which we denote k_{cat}'/K_{app}', to that in the absence of I. When equilibrium is assumed as in eq 5, $\alpha = aK_I/K_{SI} = aK_S/K_{S2}$. Within an equilibrium framework, the low values of $\alpha = 0.071$ for propidium and phenyl acetate in Figure 3b and 0.019 for propidium and acetylthiocholine in Figure 4b require either that ESI$_P$ does not form ($K_S/K_{S2} \cong 0$) or that $a \cong 0$. While these two possibilities can in principle be distinguished by analysis of the intercepts of the reciprocal plots in Figures 3a and 4a, contributions from inhibition of both acylation and deacylation complicate the interpretation (eq 5). For example, the intercepts in Figure 4b also increased with propidium concentration but in a less linear fashion than the slopes. If we denote[4] βk_{cat} as the first-order hydrolysis rate constant for the pathway through the ternary complexes ESI$_P$ and EAI$_P$, the intercept data in Figure 4b gave $\beta = 0.10$. Uncertainties in the ratio of k_2 to k_3 and in b make it difficult

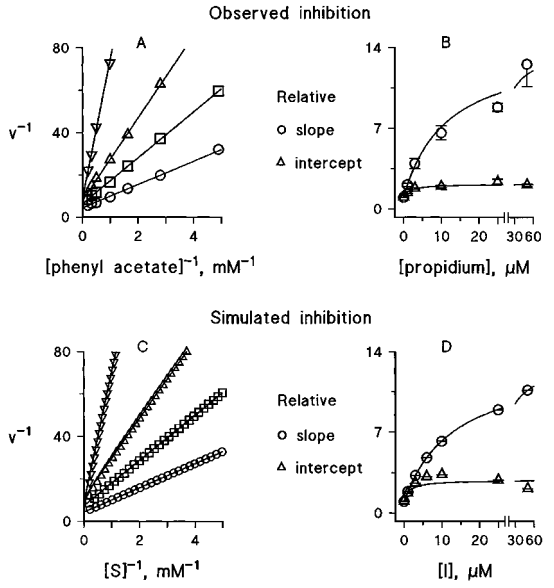

FIGURE 3: Observed and simulated inhibition of AChE-catalyzed phenyl acetate hydrolysis by propidium. Part A: Reciprocal plots of measured initial velocities (mM/min) and substrate concentrations were fitted by weighted linear regression analysis according to eq 5 at various fixed propidium concentrations ((○) 0 μM, (□) 1 μM, (△) 3 μM, (▽) 50 μM) and 0.5 nM E. Four additional points are offscale and not shown. Part B: Slopes of reciprocal plots including those in part A were normalized by dividing by K_{app}/V_{max} (the slope in the absence of propidium) and fitted by weighted nonlinear regression analysis to eq 6 to give $K_I = 0.8 \pm 0.1$ and $\alpha = 0.071 \pm 0.008$ (see Table 2). Normalized intercepts of the reciprocal plots were fitted to an equation of the same form as eq 6 to give $\beta = 0.46 \pm 0.02$ (see footnote 4 and Table 2). Part C: Plots of v^{-1} vs $[S]^{-1}$ at various [I] ((○) 0 μM; (□) 1 μM; (△) 3 μM; (▽) 50 μM) were generated by the SCoP simulation program with rate constant parameters listed for phenyl acetate and propidium in Table 2. Lines were extrapolated from linear regions of these plots encompassing $[S] = 0.02K_{app}$ to $0.2K_{app}$. Part D: Slopes and intercepts of lines calculated as in part C were analyzed by replot analysis as in part B to obtain the simulated estimates of K_I, α, and β in Table 2.

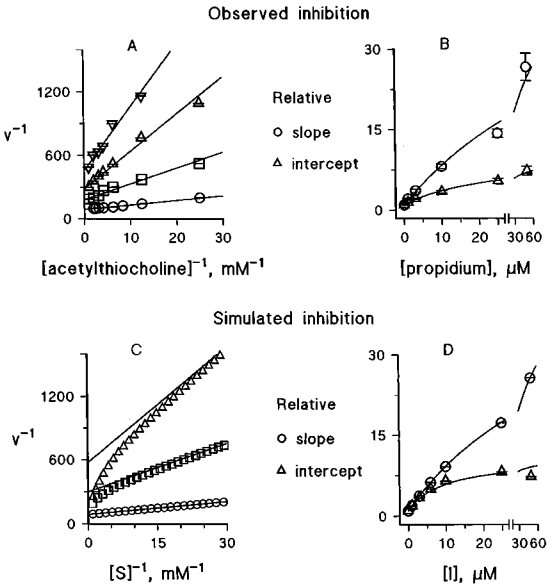

FIGURE 4: Observed and simulated inhibition of AChE-catalyzed acetylthiocholine hydrolysis by propidium. Analyses were conducted as in Figure 3. Part A: Reciprocal plots were obtained at fixed propidium concentrations ((○) 0 μM, (□) 3 μM, (△) 10 μM, (▽) 25 μM) and 25 pM E. Two additional points are offscale and not shown. Part B: Normalized slopes and intercepts of reciprocal plots including those in part A were analyzed to give $K_I = 1.1 \pm 0.1$, $\alpha = 0.019 \pm 0.004$, and $\beta = 0.10 \pm 0.01$ (see Table 1, Case 1). Part C: Plots of v^{-1} vs $[S]^{-1}$ at various [I] ((○) 0 μM; (□) 3 μM; (△) 10 μM) were generated by the SCoP simulation program with rate constant parameters listed for acetylthiocholine and propidium in Table 2. Lines were extrapolated from linear regions of these plots encompassing $[S] = 0.02K_{app}$ to $0.2K_{app}$. Part D: Slopes and intercepts of lines calculated as in part C were analyzed by replot analysis as in part B to obtain the simulated estimates of K_I, α, and β in Table 2.

to estimate a value of a from this value of β, and about all that can be concluded within this equilibrium model for propidium inhibition of acetylthiocholine hydrolysis is that a and/or b is at most 0.1. Values of β are useful, however, because they provide a basis for comparison of the experimental data with the simulated data below.

Nonequilibrium Analysis of AChE Inhibition. We noted in the Introduction that the equilibrium model assumes $k_{-S} \gg k_2$ and that this assumption does not hold for acetylthiocholine hydrolysis by AChE. Nevertheless, the rate equation in eq 5 which assumes equilibrium can still fit the observed inhibition in Figure 4. Are the mechanistic conclusions that $K_I/K_{SI} \cong 0$ or $a \cong 0$ with propidium bound to the peripheral site invalid? To address this question it is necessary to solve the rate equations for Scheme 2 without equilibrium assumptions. This solution has not been examined previously because the corresponding differential equations cannot be solved analytically. These equations can be solved numerically with the SCoP simulation program if reasonable estimates of all rate constants in Scheme 2 are available. Rate constant assignments for acetylthiocholine or phenyl acetate interaction alone with AChE were deduced as described in the Experimental Procedures and are shown in Table 1 (case 1, columns 2−4) or in Table 2. They are likely to be accurate within a factor of 2. Phenyl acetate hydrolysis by AChE also does not involve equilibrium substrate binding, and the primary difference between the assigned rate constants for acetylthiocholine and phenyl acetate was a lower value of k_S for phenyl acetate (see Experimental Procedures and footnote a in Table 2). Rate constants for propidium interaction with free AChE and the ES and EA intermediates in Scheme 2 are less certain, so we propose a simplifying hypothesis based on the location of the peripheral site at the mouth of the active site gorge. We hypothesize that the effect of propidium binding to this site is simply a steric blockade that decreases equally the association and dissociation rate constants for substrates without altering any other rate constants in Scheme 2. Thus, this steric blockade hypothesis postulates that bound propidium does not alter the thermodynamics of substrate interaction with AChE ($K_{S2} = K_S$). It also stipulates that bound propidium has no effect on acylation and deacylation rate constants ($a = b = 1$), and that bound substrate does not alter propidium interactions ($k_I = k_{SI} = k_{AI}$ and $k_{-I} = k_{-SI} = k_{-AI}$). In this case values for only the two rate constants k_I and k_{-I} for propidium interaction are required. The key feature of the hypothesis is that bound propidium slows substrate entry into and exit from the acylation site ($k_{S2} < k_S$ and $k_{-S2} < k_{-S}$). The only experimental indication to date of the extent of this slowdown involves the effect of fasciculin 2 binding to the peripheral

[4] β^{-1} is defined as the maximal factor by which the intercepts in Figure 3b increased at high concentrations of propidium. Within the equilibrium framework in eq 5, $\beta = ab(k_2 + k_3)/(ak_2 + bk_3)$ and $\beta k_{cat} = abk_2k_3/(ak_2 + bk_3)$.

site on *N*-methylacridinium binding to the acylation site: association and dissociation rate constants for *N*-methylacridinium decreased 8000- and 2000-fold, respectively, in the AChE−fasciculin 2 complex relative to those in free AChE (*27*). Steric blockade by the smaller propidium is likely to be less than that by fasciculin 2. In our simulations (Table 2 and Figures 3c and 4c) we assigned decreases in k_{S2} and k_{-S2} that gave optimal agreement with experimental data, but we also surveyed a range of decreases in these constants as described below.

The SCoP simulation procedure involved solving the set of differential equations corresponding to Scheme 2 to obtain $v = d[P]/dt$. By adjusting the total substrate and AChE amounts and the time, a series of calculated v and [S] pairs were generated as substrate was progressively converted to product at various fixed [I]. Transformation of these pairs to v^{-1} and $[S]^{-1}$ produced reciprocal plots analogous to the experimental data in Figures 3 and 4. Simulated propidium inhibition of phenyl acetate hydrolysis with k_{S2} and k_{-S2} assigned at 5% of k_S and k_{-S}, respectively, is illustrated in Figure 3c. The simulated reciprocal plots were nearly linear over a substrate concentration range corresponding to that accessible experimentally in Figure 3a. Simulated case 1 in Table 1 for propidium and acetylthiocholine, in which k_{S2} and k_{-S2} were 1.5% of k_S and k_{-S}, respectively, is illustrated in Figure 4c. The reciprocal plots were linear at low substrate concentrations, but they deviated downward at concentrations corresponding to the higher substrate concentrations examined experimentally in Figure 4a. These deviations can be eliminated if our steric blockade hypothesis is extended to include a decrease in product dissociation rate constant by bound peripheral site ligand[5] (see Discussion). However, simulations from our initial hypothesis can account for inhibition observed over the lower substrate concentrations typically employed in inhibition analyses of AChE, as the following comparisons indicate. The slopes and intercepts of the linear regions of the simulated reciprocal plots ($[S] < 0.2K_{app}$) increased as [I] became larger. The dependence of these slopes and intercepts on [I] was analyzed by nonlinear regression analyses (Figures 3d and 4d) exactly as done for the experimental data in Figures 3b and 4b. The corresponding curves (Figure 3b vs 3d and Figure 4b vs 4d) showed remarkable similarity, indicating that qualitatively our nonequilibrium hypothesis can account for inhibition of substrate hydrolysis by propidium. For a more quantitative comparison of the simulations with the experimental data, three parameters (K_I, α, and β) were examined for propidium inhibition of acetylthiocholine and phenyl acetate hydrolysis (Table 2). The K_I estimates agreed well, indicating that the K_I estimate from the simulated data still corresponds to the equilibrium constant despite the imposed nonequilibrium conditions. Furthermore, simulated α and β estimates were within about 10% of the corresponding experimental estimates for both substrates. Therefore, quantitatively as well as qualitatively, our nonequilibrium hypothesis can account for the inhibition of phenyl acetate and acetylthiocholine hydrolysis by propidium observed in Figures 3 and 4.

To demonstrate the sensitivity of the simulations to the input values, key simulation rate constants were varied and the effects on calculated values of α and β were assessed. When k_{S2} and k_{-S2} were reduced 10-fold to 0.15% of k_S and k_{-S}, estimates of α and β decreased by factors of three to six (Table 1, case 2). With k_{S2} and k_{-S2} set at 15% of k_S and k_{-S}, estimates of α and β increased to 0.18 and 0.7, respectively (data not shown), and when $k_{S2} = k_S$ and $k_{-S2} = k_{-S}$, α and β became 1.00 (Table 1, case 3). Case 3 demonstrates that, when propidium binding has no effect on any of the rate constants involving substrate hydrolysis, no inhibition is detected even though ligand binding is not at equilibrium.

Under equilibrium conditions our steric blockade hypothesis should result in no inhibition by peripheral site inhibitors. This is clear from eq 5, because the hypothesis stipulates no effect of inhibitor on either substrate binding ($K_{SI} = K_I$) or k_{cat} ($a = b = 1$). Equilibrium in Scheme 2 is approached when k_2/k_{-S} and ak_2/k_{-S2} become small. For example, if the rate constants in case 1 of Table 1 are assumed except for a 100-fold increase in k_{-S} and k_{-S2} ($k_2/k_{-S} = 0.047$ and $ak_2/k_{-S2} = 3.1$), α and β increase (Table 1, case 4) but still reflect some propidium inhibition. A further 100-fold increase in k_{-S} and k_{-S2} (to $k_2/k_{-S} = 0.00047$ and $ak_2/k_{-S2} = 0.031$) increases α to 0.97 and β to 1.00 (Table 1, case 5) and essentially abolishes the inhibition.

It is reassuring that the nonequilibrium model can account quantitatively for propidium inhibition of acetylthiocholine and phenyl acetate hydrolysis, but does this simulation model have any predictive value for the inhibition observed with other peripheral site inhibitors? Gallamine appears to bind exclusively to the peripheral site (*3*). The K_I for gallamine is 30- to 40-fold larger than the K_I for propidium (Table 2), and this lower affinity permits comparison of experimental and simulated values of α and β for a lower affinity inhibitor. The data with acetylthiocholine as substrate are shown in row 2 of Table 2, where the k_I for gallamine was assumed to be the same as that for propidium and $k_{-I} = (k_I)(K_I)$ was 30 times greater than the k_{-I} for propidium. When k_{S2} and k_{-S2} were maintained at the same values found to be optimal for propidium inhibition of acetylthiocholine hydrolysis (1.5% of k_S and k_{-S}, respectively), the simulated estimates of α and β were again within about 10% of the respective observed values. Gallamine was a less effective inhibitor of phenyl acetate hydrolysis, and the experimental and simulated values were in best accord when the simulated values of k_{S2} and k_{-S2} were 15−20% of k_S and k_{-S}, respectively (Table 2, row 4). Thus the simulations indicate that propidium or gallamine binding to the peripheral site does not reduce the rate constants of substrate association and dissociation for the neutral substrate phenyl acetate as much as for the cationic substrate acetylthiocholine.

Slow Equilibration of Acylation Site Ligands when Propidium Is Bound to the Peripheral Site. The correlation of the simulation results with experimental data in Table 2 is impressive for steady-state inhibition of both acetylthiocholine and phenyl acetate hydrolysis by propidium or gallamine. However, it is important to design additional tests of the steric blockade hypothesis that do not incorporate unknown variables such as the relative magnitudes of k_{S2} and k_S. Reversible inhibitors that equilibrate slowly with the acylation site without interfering with the peripheral site offer such a test. The interaction of an acylation site ligand (L) with AChE (*E*) in the presence of propidium (I) is shown in

[5] T. Szegletes, P. Thomas, W. D. Mallender, and T. L. Rosenberry, manuscript in preparation.

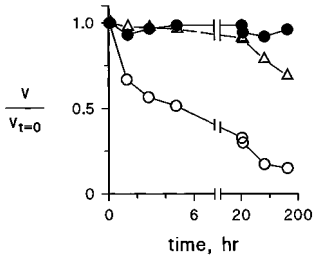

FIGURE 5: Stabilization of AChE-propidium complexes by bovine serum albumin. Incubations were conducted at 23 °C in 20 mM sodium phosphate, 0.02% Triton X-100, (pH 7.0) with (○) 1 nM AChE and 100 μM propidium; (●) 1 nM AChE, 100 μM propidium, and 1.0 mg/mL bovine serum albumin; or (△) 50 pM AChE. At the indicated times aliquots were assayed with acetylthiocholine as outlined in the Experimental Procedures. Assay points v were normalized to a control activity measured at time 0 ($v_{t=0}$). Since the inactivation was not strictly first order, lines simply connect the points. In curve (○), about 50% of the activity was lost after 6 h.

Scheme 3, where I binding to E and EL is assumed to reach equilibrium instantaneously with dissociation constants K_I

Scheme 3

$$\begin{array}{ccc} L + E & \underset{k_{-L}}{\overset{k_L}{\rightleftharpoons}} & EL \\ + & & + \\ I & & I \\ K_I \Updownarrow & & K_{LI} \Updownarrow \\ L + EI_P & \underset{k_{-L2}}{\overset{k_{L2}}{\rightleftharpoons}} & ELI_P \end{array}$$

and K_{LI}, respectively. Binding of L to E and EI_P is much slower and occurs with association rate constants k_L and k_{L2} and dissociation rate constants k_{-L} and k_{-L2}, respectively. Two acylation site ligands for which the rate constants in Scheme 3 can be measured without resorting to rapid kinetics instrumentation are huperzine A (*34*) and the transition state analogue TMTFA (*35*) (see structures in Figure 2). These ligands are also attractive because crystal structures of their complexes with AChE have been determined (see Discussion).

Before assessing the effects of propidium on the association and dissociation rate constants for these acylation site ligands, it was important to confirm AChE stability during incubation with propidium over periods of several days. Propidium in fact was observed to inactivate AChE slowly in 0.02% Triton X-100 and 20 mM sodium phosphate (pH 7.0) alone (Figure 5), but this inactivation was prevented by addition of bovine serum albumin at 1 mg/mL. It has long been known that added protein can stabilize AChE activity (e.g., gelatin; see ref *36*). However, to our knowledge this is the first report that a peripheral site ligand like propidium can promote the inactivation of AChE and that added protein can prevent this enhancement of inactivation. Bovine serum albumin was included in all subsequent experiments with acylation site ligands.

Association and dissociation rate constants for huperzine A were obtained by first determining the rate constant k for the approach to equilibrium binding at various concentrations of L and propidium according to eq 2, next resolving k_{on} and k_{off} from the dependence of k on [L] (eq 3), and then fitting k_{on} and k_{off} to eqs 4a and b. These steps are illustrated in Figure 6a−c. A family of curves showing the approach to equilibrium at several concentrations of huperzine A is shown in Figure 6a, and the k values obtained as in Figure 6a are graphed against the huperzine A concentration in Figure 6b. Estimates of k_{on} and k_{off} from plots such as that in Figure 6b at two fixed concentrations of propidium and in its absence were fitted to eqs 4a,b in Figure 6c. Rate constants obtained from this fitting procedure are given in Table 3. The decrease in the huperzine A association rate constant when propidium is bound at the peripheral site was indicated by the ratio of k_L to k_{L2}, a 49-fold decrease.

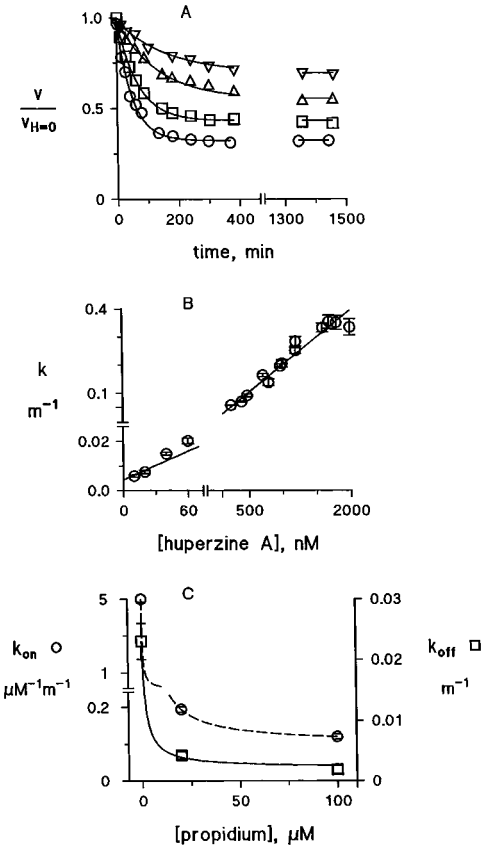

FIGURE 6: Determination of association and dissociation rate constants for huperzine A with both AChE and the AChE−propidium complex. Ligand binding was assumed to occur according to Scheme 3. Part A: Association reactions were initiated by mixing AChE (150 pM) with huperzine A ((○) 60 nM, (□) 40 nM, (△) 20 nM, (▽) 10 nM) and 20 μM propidium, and aliquots were assayed at the indicated times as outlined in the Experimental Procedures. Assay points v were normalized to a control 150 pM AChE activity with 20 μM propidium but without hyperzine A ($v_{H=0}$) and fitted to eq 2 to obtain a value of k for each curve. Part B: Values of k obtained from both part A and additional measurements at 20 μM propidium were plotted against the huperzine A concentration according to eq 3 to obtain $k_{on} = 0.195 \pm 0.007$ $\mu M^{-1}m^{-1}$ and $k_{off} = 0.0043 \pm 0.0006$ m^{-1}. In the absence of propidium, $k_{on} = k_L$ and $k_{off} = k_{-L}$ and a similar analysis was used to obtain the estimates of k_L and k_{-L} in Table 3. Part C: Values of k_{on} and k_{off} were plotted against the propidium concentration according to eqs 4a,b. The above k_L value was fixed in eq 4a, and the k_{on} estimates at 20 μM and 100 μM propidium were then fitted to this equation to obtain the estimates of k_{L2} and K_I in Table 3. Equation 4b was rearranged to the form $k_{off} = (k_{-L} + W[I]/K_I)/(1 + W[I]/K_I k_{-L2})$. The previously obtained k_{-L}, K_I, and $W = k_{L2}K_L$ were then fixed, and this equation was used to fit the k_{-L2} value in Table 3.

Table 3: Propidium Inhibition of Association and Dissociation Rate Constants for Acylation Site Ligands[a]

		acylation site ligand	
kinetic constant	units	huperzine A	TMTFA
k_L	$\mu M^{-1}\ m^{-1}$	5.0 ± 0.2	4.9 ± 0.1
k_{L2}	$\mu M^{-1}\ m^{-1}$	0.102 ± 0.009	0.013 ± 0.003
k_{-L}	m^{-1}	0.023 ± 0.003	$(2.4 \pm 0.1) \times 10^{-4}$
k_{-L2}	m^{-1}	0.0022 ± 0.0005	$(4.2 \pm 0.9) \times 10^{-6}$
K_L	nM	4.6 ± 0.7	0.049 ± 0.003
K_{L2}	nM	22 ± 5	0.32 ± 0.02
K_I	μM	0.39 ± 0.06	0.43 ± 0.05

[a] Values of kinetic constants were calculated as described in Figures 6 and 7.

Similarly, the decrease in the huperzine A dissociation rate constant when propidium is bound at the peripheral site, indicated by the ratio of k_{-L} to k_{-L2}, was about 10-fold. The steric blockade hypothesis is largely supported by these data, as both rate constants were reduced an order of magnitude or more when propidium was bound. A small thermodynamic effect of propidium binding on K_L for huperzine A, however, was also revealed by the fact that the two rate constants were not reduced equally.

The transition state analogue TMTFA has a much higher affinity for the acylation site than huperzine A. The apparent K_L of 49 pM in Table 3 is in reasonable agreement with previous estimates (*35*, *37*). This high affinity prevented application of eq 2, particularly for association reactions at low concentrations of TMTFA that were not in sufficient excess of AChE and for dissociation reactions where the free TMTFA concentration increased significantly over the course of the reaction. Therefore, several individual reaction profiles were fitted simultaneously with the SCoP program to obtain the rate and equilibrium constants in Table 3. Several of these simultaneous fits are shown in Figure 7. The reduction in TMTFA association and dissociation rate constants with propidium bound to the peripheral site was even more pronounced than for huperzine A. The association rate constant k_{L2} was 380-fold smaller than k_L with free AChE, and the dissociation rate constant k_{-L2} was 60-fold smaller than k_{-L} with free AChE. These data provide further support for the steric blockade hypothesis, again with a small thermodynamic effect of bound propidium on the TMTFA affinity.

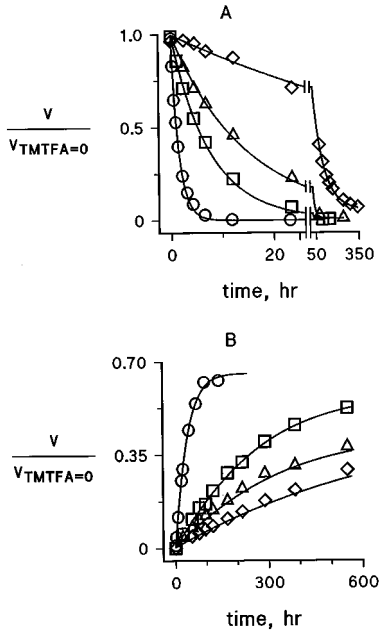

FIGURE 7: Determination of association and dissociation rate constants for TMTFA with both AChE and the AChE−propidium complex. AChE (50−800 pM) was incubated with TMTFA (0.03−320 nM) and propidium (0−100 μM) and aliquots were assayed for AChE activity at various times as outlined in the Experimental Procedures. Assay points (v) were normalized to parallel control assays ($v_{TMTFA=0}$) containing identical [AChE] and [propidium] but without TMTFA. Ligand binding was assumed to occur according to Scheme 3, and the SCoP fitting program was applied directly to the differential equations corresponding to Scheme 3. First, reaction time courses for six association and five dissociation reactions in the absence of propidium were simultaneously fit to give the values of k_L and k_{-L} in Table 3. These values were then fixed in the SCoP program and reaction time courses for five association reactions containing 100 μM propidium and eight dissociation reactions containing 20−100 μM propidium were simultaneously fit to give the values of k_{-L2}, K_{L2}, and K_I values in Table 3. Part A: Assay points and calculated fits to 4 association reactions containing 100 μM propidium, 800 pM AChE, and TMTFA (total concentration: (○) 320 nM, (□) 64 nM, (△) 33 nM, (◇) 6.4 nM). Part B: Assay points and calculated lines to four dissociation reactions containing propidium ((○) 0 μM; (□) 20 μM; (△) 40 μM; (◇) 100 μM), AChE (total concentration: (○) 62 pM, (□) 250 pM, (△) 620 pM, (◇) 620 pM), and TMTFA (total concentration: (○) 77 pM, (□) 310 pM, (△) 770 pM, (◇) 770 pM).

DISCUSSION

We illustrate here a nonequilibrium alternative to the equilibrium analysis of AChE inhibition by peripheral site ligands. We have examined a very simple hypothesis that bound peripheral site inhibitors only decrease association and dissociation rate constants for acylation site ligands *without* effects on the thermodynamics of the binding of these ligands or the rate constants for substrate acylation and deacylation. In other words, the peripheral site inhibitor is proposed to act as a "permeable cork" at the mouth of the active site "bottle" and thus to slow ligand entry to and exit from the acylation site. This steric blockade hypothesis can account for most if not all of the observed steady-state inhibition. Within an equilibrium framework, AChE inhibition by propidium previously has been attributed entirely to a conformational change at the acylation site induced by the binding of propidium to the peripheral site (*38*). This would appear reasonable in view of the spatial separation between propidium in the peripheral site and acetylthiocholine in the acylation site. According to the equilibrium model in eq 5, the low values of α and β in Figures 3b and 4b can occur only if a (or b and K_I/K_{SI}) are much less than one, and these inhibitory effects would indeed appear to require a conformational interaction between the two sites. However, the conformational interaction hypothesis fails to provide a satisfactory explanation for several observations. First, propidium only partially inhibits the hydrolysis of *p*-nitrophenyl acetate, showing an α value of about 0.3 (*39*). It is unclear why a proposed conformational interaction would result in α values ranging from less than 0.02 for a good substrate like acetylthiocholine to 0.3 for *p*-nitrophenyl acetate, but this observation is readily accommodated by the steric blockade hypothesis: For *p*-nitrophenyl acetate, the estimated K_{app} is 35-fold higher and k_{cat} is 3-fold lower than the corresponding estimates for acetylthiocholine (*39*). These values indicate that the ratios k_2/k_{-S} and ak_2/k_{-S2} are smaller for *p*-nitrophenyl acetate than for either acetylthiocholine or

phenyl acetate, placing the AChE interactions of this substrate near equilibrium where the steric blockade hypothesis predicts little inhibition. Second, in some mutants (W84A and Y130A) the K_I for propidium inhibition of acetylthiocholine hydrolysis increases up to 100-fold, while the K_{eq} for propidium binding as determined by fluorescence titration remains unchanged (*38*). In these mutants the k_{cat} for acetylthiocholine decreased 10- to 50-fold and/or K_{app} increased by more than 2 orders of magnitude (*37*, *38*), again indicating decreases in k_2/k_{-S} and ak_2/k_{-S2} that should result in less inhibition according to the steric blockade hypothesis. In fact, case 5 in Table 1 predicts no inhibition when increases in k_{-S} and k_{-S2} result in a 2000-fold increase in K_{app}, an increase comparable to the 700-fold reported for acetylthiocholine with the W84A mutant (*38*).

The simulations of steady-state substrate hydrolysis in Tables 1 and 2 provide insight into the mechanism by which peripheral site inhibition can arise within the steric blockade hypothesis. First, the ratios k_2/k_{-S} and ak_2/k_{-S2} must be large enough that the *E*S and *E*SI$_P$ complexes in Scheme 2 fail to achieve equilibrium. The k_2/k_{-S} ratio has been denoted C, the commitment to catalysis (*14*), and eq 1c shows that as C approaches and then exceeds unity the second-order substrate hydrolysis rate constant k_{cat}/K_{app} approaches k_S. According to Scheme 1, this reflects a change in the rate-limiting step from k_2 to k_S. At saturating levels of peripheral site inhibitor, the second-order substrate hydrolysis rate constant k_{cat}'/K_{app}' is given by eq 7 under equilibrium conditions and approximated by eq 7 under nonequilibrium conditions (*22*).

$$\frac{k_{cat}'}{K_{app}'} = \frac{k_{S2}ak_2}{k_{-S2} + ak_2} \qquad (7)$$

As ak_2 exceeds k_{-S2} in the *E*SI$_P$ complex, the rate-limiting step similarly becomes k_{S2}. Second, k_{S2} must be smaller than k_S. In this case, increasing saturation of the peripheral site slows the second-order hydrolysis rate constant from k_S to k_{S2}, and this slowdown is reflected in a value of $\alpha < 1$. No further restrictions on rate constants are necessary to obtain inhibition, but it is noteworthy that the relative magnitude of k_{-I} does influence the value of the inhibition parameter β, the relative value of k_{cat} in the ternary complex. The simulated β of 0.5 for gallamine inhibition of acetylthiocholine hydrolysis was significantly larger than the simulated β of 0.09 for propidium inhibition (Table 2). Since the only simulation rate constant that differed between propidium and gallamine was k_{-I}, it is clear that β was sensitive to this rate constant. For propidium k_{-I} was much less than k_2 and k_3, whereas for gallamine k_{-I} was comparable to k_2 and k_3. Thus with propidium the apparent k_{cat} is partially limited by k_{-I}, meaning that with a saturating concentration of propidium and intermediate concentrations of substrate (i.e., roughly between K_{app} and $K_{app}' \cong ak_2/k_{S2}$), most catalytic turnovers of *E*AI$_P$ are followed by slow dissociation of the *E*I$_P$ product before the next catalytic turnover. A similar effect of inhibitor dissociation rate constant on k_{cat} was noted previously for a simpler version of Scheme 2 in which *E*AI$_P$ but not *E*SI$_P$ can form (*1*, *20*). In contrast, for gallamine k_2 and k_3 alone remain largely rate limiting as in the equilibrium model in eq 5. When k_{-I} was set to a value at least 10 times k_2 or k_3 in case 1 of Table 1, β became 1.0 and k_{-I} had no influence on the relative value of k_{cat} (data not shown).

The nonequilibrium simulations in Tables 1 and 2 generated slope replots that fit eq 6 with high precision, as indicated by the low standard errors for α in Table 2. The intercept replots tended to be bell shaped rather than hyperbolic (see Figure 3d), and this led to greater uncertainty in the estimates of β. The bell-shaped curves arose from slight error that was introduced in the reciprocal plot intercepts by the curvature of the reciprocal plots that was noted in the Results in describing Figures 3c and 4c. Not all of the curvature was eliminated by restricting the simulation analyses to the low concentrations of substrate indicated. The curvature occurs because inhibition in our steric blockade model here arises exclusively from a decrease in the substrate association constant when inhibitor occupies the peripheral site ($k_{S2}/k_S \ll 1$). At high substrate concentrations with this model (i.e., as [S] approaches and exceeds $K_{app}' \cong ak_2/k_{S2}$), most catalytic turnovers of *E*AI$_P$ are followed by substrate association with *E*I$_P$ that is faster than the slow dissociation of *E*I$_P$. Hydrolysis rates approach those in the absence of inhibitor because ak_2 and bk_3 become rate limiting, and inhibitor does not affect these steps because the model sets $a = b = 1$. A logical extension of Scheme 2 consistent with the steric blockade model is to propose that bound peripheral site ligand not only reduces association and dissociation rate constants for substrate binding to the acylation site but also reduces the dissociation rate constant for product release from this site. If product affinity for the acylation site is sufficiently high, then product release may become partially rate-limiting when the peripheral site is occupied. We have found that this extension can eliminate the curvature in the reciprocal plots and give quantitative agreement between simulated and experimental data over the entire range of substrate concentrations. Furthermore, if substrate can form a low affinity complex at the peripheral site and block product dissociation from the acylation site, this extended model can account quantitatively for substrate inhibition.[5] The necessity for slight revision of the simplest version of the steric blockade hypothesis offered here also is indicated by consistent observations of small decreases in the affinity of ligands in ternary AChE complexes relative to the corresponding binary complex. In Table 3 this decrease, indicated by the ratio of K_{L2}/K_L, was a factor of 4.7 ± 1.4 for huperzine A and of 6.5 ± 0.6 for TMTFA in the AChE−propidium complex relative to the free enzyme. Other studies have shown an affinity decrease of about 5 for edrophonium (*22*) and 4 for methylacridinium (*27*) in the AChE−fasciculin 2 complex relative to free AChE. The consistent magnitude of these factors suggests that affinity decreases of cationic ligands in many AChE ternary complexes are governed by general properties such as electrostatic attraction rather than specific conformational interaction. Even though the steric blockade hypothesis here proposed no changes in equilibrium constants in AChE ternary complexes, a minor 5-fold decrease in ligand affinities in the ternary complexes can be incorporated into the hypothesis with virtually no effect on simulated values of α and β. For example, a 5-fold increase in k_{-S2} and k_{-SI} from their values in case 1 of Table 1 changes the simulated values of α and β by less than 8% (data not shown).

Despite the agreement of the simulated and experimental data for the two substrates and two inhibitors in Table 2, these data provide only a correlation and do not prove our

nonequilibrium steric blockade hypothesis. The predictive power of the hypothesis would be enhanced if *all* the rate constants in the simulations could be assigned independently, but independent estimates of k_{S2} and k_{-S2} for substrates are very difficult to obtain. Alternatively, the hypothesis predicts that not only substrates but also ligand inhibitors that bind to the acylation site should show decreased association and dissociation rate constants (k_{L2} and k_{-L2}) when a peripheral site ligand like propidium is bound. Most acylation site ligands equilibrate too rapidly to test this prediction. For example, *N*-methylacridinium has a K_I in the micromolar range and equilibrates with AChE in about a msec or less (*27*, *40*). However, huperzine A binds near the acylation site (*28*) and equilibrates slowly enough to allow measurement of association and dissociation rate constants (*34*). Furthermore, the AChE complex with the trifluoromethyl ketone TMTFA provides an excellent model of the transition state for acylation by acetylcholine. The crystal structure of the TMTFA−TcAChE complex shows a tetrahedral adduct that nearly superimposes on a calculated structure of acetylcholine in the active site (*29*). TMTFA has no leaving group, so it accumulates as the tetrahedral adduct. Molecular modeling of the ternary complexes of these ligands with TcAChE−propidium revealed that the bound propidium is separated by at least 1.6 Å from either bound huperzine A or bound TMTFA (Figure 8), indicating that no overlap occurs in the binding sites that could perturb equilibrium affinities in the ternary complexes. As noted above in support of this conclusion, the 4- to 7-fold decreases in ligand equilibrium affinities in these ternary complexes are comparable to those reported previously for ternary complexes involving fasciculin 2 in the peripheral site. Measured values of k_{L2} and k_{-L2} for huperzine A and TMTFA with the AChE−propidium complex provide compelling support for our steric blockade hypothesis. These rate constants are 49- and 10-fold lower for huperzine A and 380- and 60-fold lower for TMTFA than the respective rate constants k_L and k_{-L} for the interaction of these ligands with free AChE. It is particularly satisfying that the magnitude of these decreases for the acetylcholine analogue TMTFA agrees so well with the simulated k_S/k_{S2} ratio of about 70 that was found to provide the best correspondence to observed kinetic parameters for acetylthiocholine and propidium in Table 2.

Does the successful application of our steric blockade hypothesis in this report rule out any conformational interaction between the peripheral and acylation sites? We argue that it probably does when the peripheral site is occupied by small ligands such as propidium and gallamine. Proof of this conformational interaction now requires evidence beyond steady-state measurements of the extent of propidium inhibition. For example, with the larger ligand fasciculin 2 bound to the peripheral site, we previously reported not only steric blockade of ligand access to the acylation site (*27*) but also a conformational change in the acylation site that decreased the efficiency of the catalytic triad (*22*). This additional conformational effect of bound fasciculin is seen most clearly by comparing estimates of the dissociation rate constant k_{-L2} for TMTFA. In contrast to the 60-fold decrease in this rate constant observed here for the AChE−propidium−TMTFA complex relative to k_{-L} for AChE-TMTFA, a 20-fold *increase* in k_{-L2} relative to k_{-L} was reported for the AChE-fasciculin 2-TMTFA complex (*37*).[6] The increase results in conformational destabilization of the tetrahedral TMTFA adduct in this ternary complex ($K_{L2}/K_L \cong 200$), and the conformational effect predominates over steric blockade of TMTFA egress in determining the net change in k_{-L2}. Crystal structure analyses of fasciculin-AChE complexes (*8*, *9*) show that fasciculin 2 interacts not only with W279 in the peripheral site but also with residues on the outer surface of an ω-loop within 4 Å of W84 in the acylation site, well beyond the region of the peripheral site occupied by propidium (see Figures 7 and 8). These more extensive surface interactions provide a structural basis for an inhibitory conformational effect on the acylation site when fasciculin rather than propidium is bound to the peripheral site.

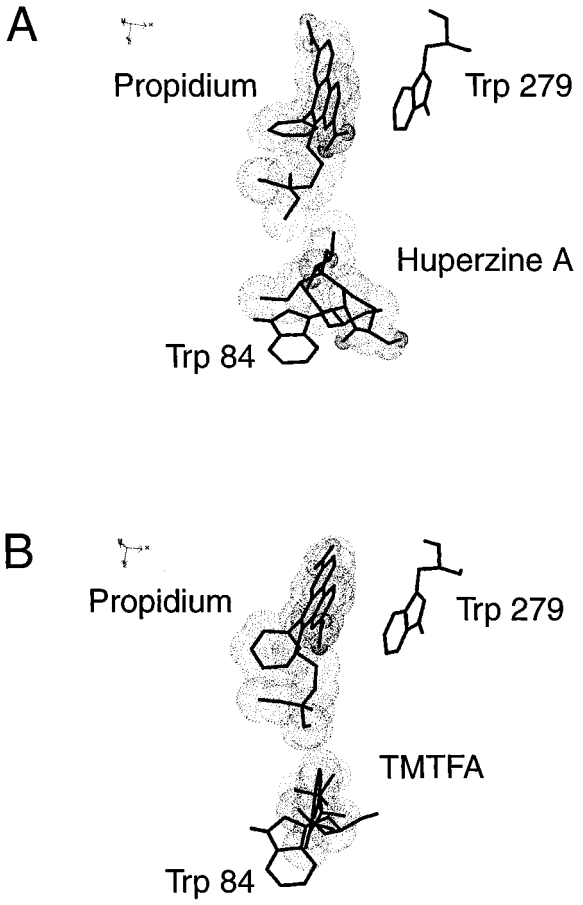

FIGURE 8: Molecular models of ternary complexes involving propidium and TcAChE. Residues are marked by a heavy line with propidium and acylation site ligand van der Waals spheres shown by a dotted surface. Nonpolar hydrogen atoms have been omitted for clarity. The conformation of propidium in the TcAChE−huperzine A complex (part A) was very similar to that in the TcAChE−TMTFA adduct (part B). The overall root mean square deviation between matched atoms in the two models was 0.25 Å. Atom to atom closest contacts between the propidium alkyl chain and the acylation site inhibitors are 1.6 Å (huperzine A) and 1.7 Å (TMTFA). Comparison of the propidium molecule between the two models revealed only minor changes in both the planarity of the aromatic ring and the position of the alkyl chain.

ACKNOWLEDGMENT

We express our gratitude to Dr. Michel Roux at the Ecole Normale Superieure in Paris, France, for bringing the SCoP

[6] J. Eastman, P. Thomas, G. Rogers, J. Yustein, and T. L. Rosenberry, unpublished observations.

program to our attention. We also acknowledge the technical assistance of Mr. Mark Frey in early measurements of propidium inhibition of substrate hydrolysis and thank Dr. Daniel Quinn in the Department of Chemistry at the University of Iowa for kindly supplying TMTFA.

REFERENCES

1. Rosenberry, T. L. (1975) Acetylcholinesterase, in *Advances in Enzymology* (Meister, A., Ed.) Vol. 43, pp 103−218, John Wiley & Sons, New York.
2. Sussman, J. L., Harel, M., Frolow, F., Oefner, C., Goldman, A., Toker, L., and Silman, I. (1991) *Science 253*, 872−879.
3. Taylor, P., and Lappi, S. (1975) *Biochemistry 14*, 1989−1997.
4. Weise, C., Kreienkamp, H.-J., Raba, R., Pedak, A., Aaviksaar, A., and Hucho, F. (1990) *EMBO J. 9*, 3885−3888.
5. Schalk, I., Ehret-Sabatier, L., Bouet, F., Goeldner, M., and Hirth, C. (1992) in *Multidisciplinary Approaches to Cholinesterase Functions* (Shafferman, A., and Velan, B., Eds.) pp 117−120, Plenum Press, New York.
6. Radic, Z., Pickering, N. A., Vellom, D. C., Camp, S., and Taylor, P. (1993) *Biochemistry 32*, 12074−12084.
7. Barak, D., Kronman, C., Ordentlich, A., Ariel, N., Bromberg, A., Marcus, D., Lazar, A., Velan, B., and Shafferman, A. (1994) *J. Biol. Chem. 269*, 6296−6305.
8. Harel, M., Kleywegt, G. J., Ravelli, R. B. G., Silman, I., and Sussman, J. L. (1995) *Structure 3*, 1355−1366.
9. Bourne, Y., Taylor, P., and Marchot, P. (1995) *Cell 83*, 503−512.
10. Karlsson, E., Mbugua, P. M., and Rodriguez-Ithurralde, D. (1984) *J. Physiol. (Paris) 79*, 232−240.
11. Marchot, P., Khelif, A., Ji, Y.-H., Masnuelle, P., and Bourgis, P. E. (1993) *J. Biol. Chem. 268*, 12458−12467.
12. Nachmansohn, D., and Wilson, I. B. (1951) *Adv. Enzymol. 12*, 259−339.
13. Briggs, G. E., and Haldane, J. B. S. (1925) *Biochem. J. 19*, 338−339.
14. Quinn, D. M. (1987) *Chem. Rev. 87*, 955−979.
15. Dixon, M., and Webb, E. C. (1958) *Enzymes*, pp 171−181, Academic Press, New York.
16. Rosenberry, T. L., and Scoggin, D. M. (1984) *J. Biol. Chem. 259*, 5643−5652.
17. Roberts, W. L., Kim., B. H., and Rosenberry, T. L. (1987) *Proc. Natl. Acad. Sci. U.S.A. 84*, 7817−7821.
18. Riddles, P. W., Blakeley, R. L., and Zerner, B. (1979) *Anal. Biochem. 94*, 75−81.
19. Ellman, G. L., Courtney, K. D., Andres, J. V., and Featherstone, R. M. (1961) *Biochem. Pharmacol. 7*, 88−95.
20. Hodge, A. S., Humphrey, D. R., and Rosenberry, T. L. (1992) *Mol. Pharmacol. 41*, 937−942.
21. Rosenberry, T. L. (1975) *Proc. Natl. Acad. Sci. U.S.A. 72*, 3834−3838.
22. Eastman, J., Wilson, E. J., Cervenansky, C., and Rosenberry, T. L. (1995) *J. Biol. Chem. 270*, 19694−19701.
23. Hindmarsh, A. C. (1983) in *Scientific Computing* (Stepleman, R. S., et al., Eds.) pp 55−64, North-Holland, Amsterdam.
24. Petzhold, L. R. (1983) *SIAM J. Sci. Stat. Comput. 4*, 136−148.
25. Froede, H. C., and Wilson, I. B. (1984) *J. Biol. Chem. 259*, 11010−11013.
26. Gnagey, A. L., Forte, M., and Rosenberry, T. L. (1987) *J. Biol. Chem. 262*, 13290−13298.
27. Rosenberry, T. L., Rabl, C. R., and Neumann, E. (1996) *Biochemistry 35*, 685−690.
28. Raves, M. L., Harel, M., Pang, Y.-P., Silman, I., Kozikowski, A. P., and Sussman, J. L. (1997) *Nat. Struct. Biol. 4*, 57−63.
29. Harel, M., Quinn, D. M., Nair, H. K., Silman, I., and Sussman, J. L. (1996) *J. Am. Chem. Soc. 118*, 2340−23346.
30. Botts, J., and Morales, M. (1953) *Trans. Faraday Soc. 49*, 696−707.
31. Bernhard, S. A. (1968) The Structure and Function of Enzymes, in *Biology Teaching Monograph Series* (Levinthal, C., Ed.) pp 80−85, W. A. Benjamin, Inc., New York.
32. Krupka, R. M., and Laidler, K. J. (1961b) *J. Am. Chem. Soc. 83*, 1454−1458.
33. Barnett, P., and Rosenberry, T. L. (1977) *J. Biol. Chem. 252*, 7200−7206.
34. Ashani, Y., Grunwald, J., Kronman, C., Velan, B., and Shafferman, A. (1994) *Mol. Pharmacol. 45*, 555−560.
35. Nair, H. K., Lee, K., and Quinn, D. M. (1993) *J. Am. Chem. Soc. 115*, 9939−9941.
36. Wilson, I. B., and Bergmann, F. (1950) *J. Biol. Chem. 185*, 479−489.
37. Radic, Z., Quinn, D. M., Vellom, D. C., Camp, S., and Taylor, P. (1995) *J. Biol. Chem. 270*, 20391−20399.
38. Barak, D., Ordentlich, A., Bromberg, A., Kronman, C., Marcus, D., Lazar, A., Ariel, N., Velan, B., and Shafferman, A. (1995) *Biochemistry 34*, 15444−15452.
39. Ordentlich, A., Barak, D., Kronman, C., Flashner, Y., Leitner, M., Segall, Y., Ariel, N., Cohen, S., Velan, B., and Shafferman, A. (1993) *J. Biol. Chem. 268*, 17083−17095.
40. Rosenberry, T. L., and Neumann, E. (1977) *Biochemistry 16*, 3870−3878.

BI972158A